Molecular dynamics simulation of microwave heating and collapse of methane hydrate by TIP5P-Ewald water model

Motohiko Tanaka
Innovative Energy Science and Engineering, Chubu University, Japan.

November 3, 2023

Abstract

Microwave heating of methane hydrate is studied with electrostatic molecular dynamics simulations by the five-body Coulomb and TIP5P-Ewald water model. The structure I of methane hydrate is constructed. When the methane hydrate of density 0.91 $\mathrm{g/cm^3}$ and a temperature 273 K is exposed to microwave electric fields of 10 GHz, it suddenly collapses to become liquid after a certain period of irradiation. The period of a collapse time is $1.7\times10^6\tau$ and the temperature increase is $\Delta T\cong 61$ degrees, where the external electric field is $3\times10^7\mathrm{V/cm}$ (i.e. 0.3 V/Å) and $\tau=1\times10^{-14}$ s.

Subjects: Chemical Physics (physics.chem-ph)
http://www1.m4.mediacat.ne.jp/dphysique/

1 Introduction

The natural gas resources of methane hydrate that are found in permafrost and the sea floor of the earth may be drawing public attention [1]. The production of methane from methane hydrate, however, contributes much more than carbon deoxide to greenhouse effects [2, 3]. Methane hydrate is a solid or liquid material and is a light electrolyte like ice. It has a density of 0.91 $\mathrm{g/cm^3}$ at an atmospheric pressure and 0.95 $\mathrm{g/cm^3}$ for an elevated pressure of 50 atm. Methane hydrate dissociates to about 220 ml of methane gas against 1 g water at 1 atm and 273 K. It is stable at pressures higher than 0.1 MPa at 193 K and 2.3 MPa at 273 K.

There are three states of methane hydrates [1, 4]. System I has 46 H_2O molecules that form 5^12 and $5^{12}6^2$ cages containing the guest molecules CH_4 and CO_2. System II has 136 H_2O molecules that form 5^{12} and $5^{12}6^4$ tetragonal cages containing oxygen and other molecules. Both systems have cubic lattices. The hexagonal system H has 5^{12}, $5^{12}6^{16}$, and $4^35^66^3$ polyhedron cages of the C_6H_{14} molecules, which exist as a hexagonal lattice.

High-pressure experiments on methane hydrate have been performed using a diamond-anvil cell [5]. Experiments below the melting point of ice surveyed energetically for hydrates. The stability of hydrates in the thermodynamic instability region of the ice Ih clathrate has been discussed [6]. Many traditional equations of state have been utilized to describe thermo-physical properties and

phase equilibrium [7]. The multi-scale phase diagram of the Gibbs-Helmholtz constrained equation of state for methane hydrate has been tabulated by density for given pressures and temperatures [8, 9].

The diffusion coefficients and dielectric relaxation properties of water, i.e., the response of electric dipoles to a given initial impulse, have been studied theoretically [10]. The heating and diffusion of water under high-frequency microwaves and infrared electromagnetic waves have been investigated by molecular dynamics simulations using elaborated point-charge models [11]. Molecular dynamics simulation of the ice nucleation and growth process leading to water freezing has been executed [12]. Molecular dynamics simulations have been conducted concerning the microwave heating of water, ice, and saline solution [13].

Molecular dynamics employing the density functional method (DFT) to simulate the THz range of electromagnetic wave have been constructed [14]. They have shown, by the self-consistent atomic forces [15], that: (i) liquid water molecules in the electric field has excited rotational motions, as water molecules in the cages can not make free translation motions; (ii) the electron energy is about twice the kinetic energy of the water molecules, which results from the forced excitation of the molecules by the electromagnetic THz external field.

An important question arises concerning heating of the methane hydrates. Could heating by microwaves be continued as a crystal or liquid beyond 273 K ? The rest of this paper is organized as follows. The methodology of electrostatic molecular dynamics with equation of motion and procedures of the model are given in Section 2. Modeling of present simulations is given in Section 3.1, and heating and collapse of methane hydrate are shown in Section 3.2. A summary is provided in Section 4. The equations of long-range Coulombic interactions are explained in Appendix A.

2 Methodology of Molecular Dynamics

2.1 Equation of Motion and Forces

Crystal structures are a part of the solid-state physics [16]. Four basic quantities are used to derive the Newtonian equation of motion for water molecules: the time $\tau = 1 \times 10^{-14}$ s, the length 1 Å= 1×10^{-8} cm, mass of water $M_0 = 3.0107 \times 10^{-23}$ g, and electronic charge $e = 4.8033 \times 10^{-10}$ esu (1.6022×10^{-19} C in the international units system). Then, one has the equations [13, 17],

$$M_i \frac{d\vec{v}_i}{dt} = -\nabla \left\{ \Phi_F(\vec{r}_i) + \left[A/r^{12} - B/r^6 \right] \right\} + q_i E \sin \omega t \, \hat{x}, \tag{1}$$

$$\frac{d\vec{r}_i}{dt} = \vec{v}_i. \tag{2}$$

that define the equations of motion. The first term of the right-hand side of Eq.(1) is the Coulombic potential $\Phi_F(\vec{r}_i)$, and the second term is the Lennard-Jones potential. Here, $\vec{r}_i$ and $\vec{v}_i$ are the position and velocity of i-th molecule, respectively, M_i and q_i are the mass and charge, respectively, t is the time, and ∇ is the space derivative. The quantity $\vec{r}_{ij} = \vec{r}_i - \vec{r}_j$ is the particle spacing between the i-th and j-th molecules. A and B are the coeffcients of Lennard-Jones potential, respectively, with $A = 4\varepsilon\sigma^{12}$ and $B = 6\varepsilon\sigma^6$ where ε is the depth of the potential well and σ is the distance at which the particle potential energy bocomes zero.

The external electric field E points to the x direction and has the sinusoidal form $\sin \omega t$ where the frequency f is $\omega = 2\pi f$. The time step is $\Delta t = 0.025\tau$ (i.e., 2.5×10^{-16}s). In a time marching fashion, the current step of $\vec{r}_i$ and $\vec{v}_i$ is forwarded to the next time step. When a sufficient amount of time has elapsed, one analyzes the time development.

To represent the crystal system with high accuracy, one has to separate the Coulombic forces $\vec{F}(\vec{r}_i) = -\nabla\Phi_F(\vec{r}_i)$ that occur in the short-range and the long-range interactions [18, 19, 20],

$$\vec{F}(\vec{r}_i) \quad = \quad \vec{F}_{SR}(\vec{r}_i) + \vec{F}_{LR}(\vec{r}_i). \tag{3}$$

The short-range interactions are written as,

$$\vec{F}_{SR}(\vec{r}_i) \quad = \quad \sum_{j=1}^{N} q_i q_j \Big[\Big(\frac{\mathrm{erfc}(r_{ij})}{r_{ij}} + \frac{2\alpha}{\sqrt{\pi}} \Big) \exp(-(\alpha r_{ij})^2)/r_{ij}^2 \Big] \vec{r}_{ij}, \tag{4}$$

where the Gauss complimentary error function is

$$\mathrm{erfc}(r) = \frac{2}{\sqrt{\pi}} \int_r^{\infty} \exp(-t^2) dt. \tag{5}$$

The α value, a minimization factor, is discussed later.

A primary factor in the long-range interactions is the charge density, $\rho(\vec{r}_i) = \sum_j q_j S(\vec{r}_i - \vec{r}_j)$, which is the near-site grid sum with $S(\vec{0}) = 1$, $S(\infty) \to 0$. Then, the grid summation is converted to the k-space by a Fourier transform $FT^{-1}[...]$. Here, $\rho(\vec{r}) \to \rho_k(\vec{k})$ with $\vec{k} = 2\pi\vec{n}/L$, n the integers ≥ 0, and L the length. The inverse Fourier transform to return to the coordinate space is executed by the folding operations $FT[...]$,

$$\vec{F}_{LR}(\vec{r}_i) \quad = \quad -FT\Big[i\, q_i(dn(n_x), dn(n_y), dn(n_z)) G(n_x, n_y, n_z)\ \rho_k(\vec{k}) \Big], \tag{6}$$

$$dn(n_\gamma) = n_\gamma - dnint(n_\gamma/M_\gamma) M_\gamma \quad (\gamma = x, y, z). \tag{7}$$

The expressions for the $G(n_x, n_y, n_z)$, $\vec{K}(n_x, n_y, n_z)$ and $\Delta(n_x, n_y, n_z)$ functions are given in Appendix A. The α value is determined by minimizing the errors of both the short-range and long-range interactions of the electric fields [21]. The value is $\alpha = 0.203$ for the total number of 3^3 methane hydrates.

The five-point molecules are used for water which is known as the TIP5P-Ewald model. A four-water molecule is specified to calculate positive two hydrogens $q_H = 0.241e$ and negative two hydrogens $q_L = -0.241e$ with e the electron charge. The angle and bond are $\psi_1 = 104.52^\circ$, $r = 0.9572$ Å for the H site and $\psi_2 = 109.47^\circ$, $r = 0.7$ Å for the L site. The fifth oxygen atom called the dummy site $q_O = 0$ is to correlate with adjacent molecules using the Lennard-Jones potential $\Psi(r) = A/r^{12} - B/r^6$. The factors of the TIP5P-Ewald water model are $A = 3.8538 \times 10^{-8}$ erg Å^{12} and $B = 4.3676 \times 10^{-11}$ erg Å^6 [22]. The classic mechanics and related topics are written in the Goldstein's book [23].

2.2 Procedures of Five-Body Water Molecules

The important points of the five-body molecules are first summarized.
A. Five sites are one oxygen of O site, hydrogens of H_1 and H_2, and negative hydrogen virtual sites of L_1 and L_2. Their charges are 0, $0.241e$, $0.241e$, $-0.241e$ and $-0.241e$, respectively. The L_1 and L_2 are called the dummy sites.
B. Separate the translational part $\boldsymbol{R}_j$, $\boldsymbol{V}_j$ for molecules ($j = 1, N/5$), where the rotation part $\boldsymbol{r}_i = (x_i, y_i, z_i)$ ($i = 1, N$) for atoms is used for the five sites. The separation is done at the starting step only; once determined at $t = 0$, they become constant in time.
C. The half time step for the molecules is first executed for a predictor step, and next the full time step is made for advancement of time.
D. Before the end of the step, the forces are calculated by atom positions, where the dummy L sites are obtained by algebraic vector operation.
E. After correction of quaternions, the kinetic and Coulombic energies are calculated, and go to the beginning of the cycle. The leap-frog method is used for the plasmas and water.

Each step of the cycle corresponds to (i) translational motion (Step 1), (ii) rotational motion (Step 2-4), and (iii) addition of the fields (Step 5-8).
0) Read positions $\boldsymbol{r}_i$ and quaternions $\boldsymbol{q}_j$ from files by "$read(17)\ x_i, y_i, z_i$" ($i = 1, N$), where the dummy sites are obtained by algebraic vector operation. Also, "$read(30)\ e_{0j}, e_{1j}, e_{2j}, e_{3j}$" ($j = 1, N/5$). This step is executed only at the first time.
1) The position $\boldsymbol{R}_j$ and velocity $\boldsymbol{V}_j$ of each molecule ($j = 1, N/5$) are advanced by summation over five sites of forces $\boldsymbol{F}_k$ ($k = 1, N$) for the translational motion,

$$d\boldsymbol{V}_j/dt = (1/m_j)\sum_{k=1}^{5} \boldsymbol{F}_k, \quad d\boldsymbol{R}_j/dt = \boldsymbol{V}_j. \tag{8}$$

2) Next steps of 2) to 5) are made for half a time steps $\Delta t_1 = \Delta t/2$ by prediction, and then for a full time step $\Delta t_2 = \Delta t$ by correction. The angular momentum of rotational motion is calculated at a time step Δt_1 or Δt_2 by summation over the torque of five sites,

$$d\boldsymbol{L}_j/dt_n = \sum_{k=1}^{5} (y_k F_k^z - z_k F_k^y, z_k F_k^x - x_k F_k^z, x_k F_k^y - y_k F_k^x) \tag{9}$$

3) The angular frequency $\omega_{j,\alpha}$ is connected to the angular mementum and inertia moment $Im_{j,\alpha}$ with $\alpha = x, y, z$ and the matrix $A_{\alpha,\beta}$ are,

$$\omega_{j,\alpha} = (A_{\alpha 1} L_x + A_{\alpha 2} L_y + A_{\alpha 3} L_z)/Im_{j,\alpha} \tag{10}$$

$$\begin{array}{lll} A_{11} = e_0^2 + e_1^2 - e_2^2 - e_3^2, & A_{12} = 2(e_1 e_2 + e_0 e_3), & A_{13} = 2(e_1 e_3 - e_0 e_2), \\ A_{21} = 2(e_1 e_2 - e_0 e_3), & A_{22} = e_0^2 - e_1^2 + e_2^2 - e_3^2, & A_{23} = 2(e_2 e_3 + e_0 e_1), \\ A_{31} = 2(e_1 e_3 + e_0 e_2), & A_{32} = 2(e_2 e_3 - e_0 e_1), & A_{33} = e_0^2 - e_1^2 - e_2^2 + e_3^2, \end{array} \tag{11}$$

4) The time derivative of quaternion $\boldsymbol{q}_j = (e_0, e_1, e_2, e_3)$ is given by the angular frequency by,

$$d\boldsymbol{q}_j/dt_n = (1/2)\Delta t_n \begin{pmatrix} -e_1\omega_x - e_2\omega_y - e_3\omega_z \\ e_0\omega_x - e_3\omega_y + e_2\omega_z \\ e_3\omega_x + e_0\omega_y - e_1\omega_z \\ -e_2\omega_x + e_1\omega_y + e_0\omega_z \end{pmatrix} \tag{12}$$

5) Get a rotation matrix $A_{\alpha\beta}(e_0,e_1,e_2,e_3)$ in half a time steps for prediction and go back to Step 2. In the correction step, it is made for a full time step and go to Step 6.
6) The three sites $\boldsymbol{r}_i$ and the position $\boldsymbol{R}_j$ are connected by,

$$\boldsymbol{r}_i = \boldsymbol{R}_j + \begin{pmatrix} A_{11} & A_{21} & A_{31} \\ A_{12} & A_{22} & A_{32} \\ A_{13} & A_{23} & A_{33} \end{pmatrix} \begin{pmatrix} x_i \\ y_i \\ z_i \end{pmatrix} \tag{13}$$

The positions of dummy sites L_1 and L_2 are calculated from known three sites of O, H_1 and H_2 by algebraic vector operation.
7) The forces of positions are calculated from Coulombic and Lennard-Jones potentials using the five sites.
8) Correction to a normalization of quaternions is made at every 10 steps, and go to the new time step of Step 1.

Note that a time step is important and it will be $\Delta t = 0.025\tau$ or less by the time advancing scheme; otherwise the code will be inaccurate or go to overflow.

Table 1: The run series, fixed density ($\mathrm{g/cm^3}$), electric field (V/Å), microwave heating rate (W_0/τ) with W_0 the initial kinetic energy of methane hydrate, heating time before collapse, and guests molecules for the constant volume case.

series	density	E	heating rate	heating time	guests molecules
A1	$0.91\mathrm{g/cm^3}$	0.30 V/Å	$3.0\times10^{-7}W_0/\tau$	$1.7\times10^{6}\tau$ collapsed	CH_4
A2	$0.91\mathrm{g/cm^3}$	0.40 V/Å	$3.7\times10^{-5}W_0/\tau$	$6.3\times10^{4}\tau$ collapsed	CH_4

3 Simulations of Methane Hydrate

3.1 Modeling

To represent electrostatic effects for water molecules, one can adopt the three-body model [24, 25], and various four-body to five-body models [26]. Although the three-body model has a lower temperature problem than the real one, it has an explicit stable scheme in the coordinate space [27]. The microwave heating and collapse of methane hydrate were studied by the three-body model [28]. Nowaday the five-body models are used, but there occurs a unrealistic drift to increase the kinetic energy with a time rate $W_{dr}/\tau = 1.6\times10^{-7}W_0/\tau$ for the null external electric field. The kinetic energy of Run A's in Table 1 are already subtracted.

The initial structure of methane hydrate is installed by the Genice program on the Linux system [29]. The size of structure I methane hydrate has about 12 Å as the crystal structure. A total of 3^3 methane hydrates exists in the three-dimensional water system. The Lennard-Jones potential parameter for water was argued in Sec.2.2. A system of guest molecules of CH_4 which are the united atoms is used for the Lennard-Jones potential in the second term on the righthand side of Eq.(1). ε_{ij} and σ_{ij} are the two-particle interaction potential and the radius of the molecule, respectively, and

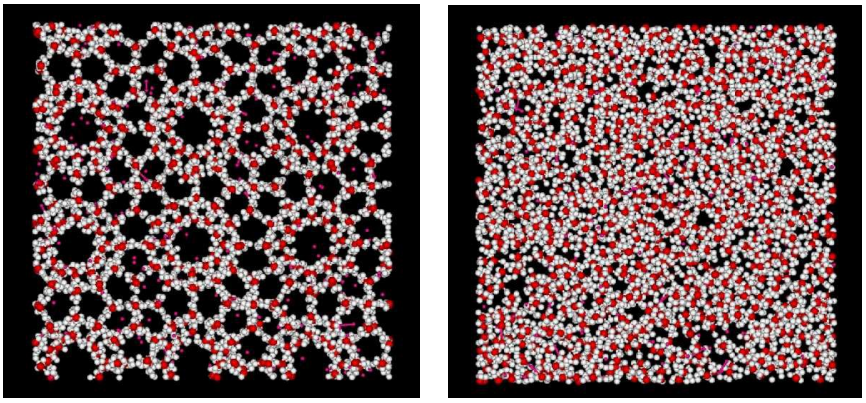

Figure 1: (Left) Methane hydrate of the H (white), O (red), and CH_4 (small red) molecules having a density of 0.91 g/cm^3 before collapse at the time $t = 1.65 \times 10^6 \tau$, (Right) Distortion of the methane hydrate in liquid under an applied microwave field observed at $t = 1.70 \times 10^6 \tau$.

the potential coefficient is $\varepsilon_{CH_4} = 0.39$ kJ/mol and its radius is $\sigma_{CH_4} = 3.82$ Å [30]. In order to perform the molecular dynamics simulation, the frequency is set to 10 GHz ($f = 2\pi \times 10^4/\tau$). The external electric field is 0.3V/Å for Run A1 and 0.4V/Å for Run A2.

3.2 Heating and Collapse of Methane Hydrate

The heating of methane hydrates is done under the application of microwave fields. In the heating described, the volume is assumed to be constant. The hydrate used in this simulation is a normal pressure case (1 atm, Run A's), and the density is 0.91 g/cm^3 [1, 9]. The run has an initial temperature of 273 K of the crystal.

The kinetic energy of the water molecule is $W_s = (1/2)M_0\vec{V}_s^2 + (1/2)I\omega^2$, where $\vec{V}_s$ and I, respectively, are its velocity and moment of inertia. The translational and rotational motions are included for the water molecules. The mass of water $M_{\mathrm{H_2O}}$ is set to unity and $\vec{V}_{s0}$ is the initial velocity.

Microwaves are applied in Run A1. With the microwave electric field on, the kinetic energies of the water and CH_4 molecules increase over time, but the water and CH_4 (unified atom) molecules are the same up to the left panel of Fig.1. The nonlinear growth of methane hydrate occurs for the early time $t > 5 \times 10^5 \tau$. The increase in the energy of the water is $W/\tau \cong 3.0 \times 10^{-7} W_0/\tau$. The CH_4 molecules, without any charges, are inert to microwaves, but they interact with water molecules. The energy increases in the Lennard-Jones potential, which was close to the water case. The temperature increase before the microwave collapse for Run A1 is $\Delta T \cong 61$ degrees. The total energy of the kinetic energies of water and CH_4 become very large at $t > 1.7 \times 10^6 \tau$, as depicted in Fig.2. The explosive growth suddenly collapses, and the Lennard-Jones energy decreases chaotically. Methane hydrate turns to be the liquid phase, as the right panel of Fig.1.

The pair distribution functions of the O-O and O-H atoms are shown in Fig.3 for the methane hydrate with a density of 0.91g/cm^3. Their times are corresponding to before and after the collapse

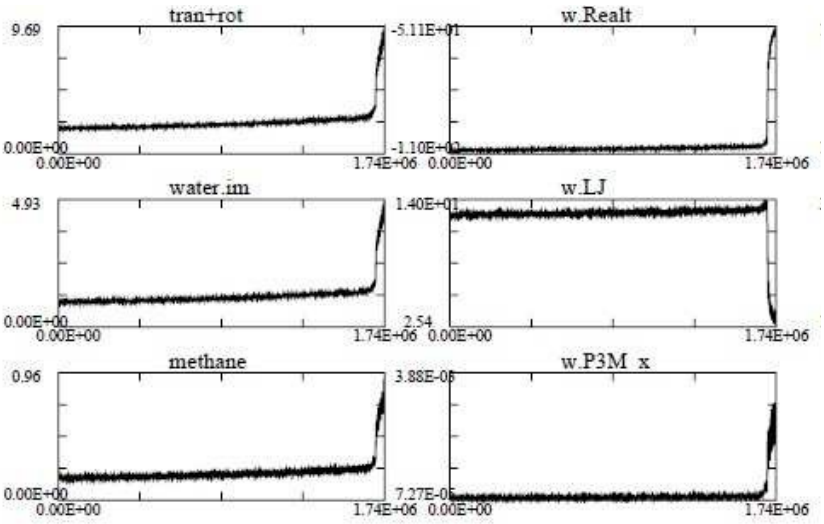

Figure 2: Microwaves are applied to methane hydrate with density of 0.91 g/cm^3 and temperatures at $T \geq 273$ K. Left: The kinetic energy of translation+rotation, that of rotation, that of CH_4 (top to bottom, respectively). Right: The short-range Coulomb interaction energy, the Lennard-Jones potential energy, and P3M energy (top to bottom, respectively). The abscissa is linearly scaled in all plots. The kinetic energy of water increases with a time rate of $W/\tau = 3.0 \times 10^{-7} W_0/\tau$, and the short and long-range energies eventually collapse to be liquid at the time $t \cong 1.7 \times 10^6 \tau$, whereas the Lennard-Jones energy decreases at the same time.

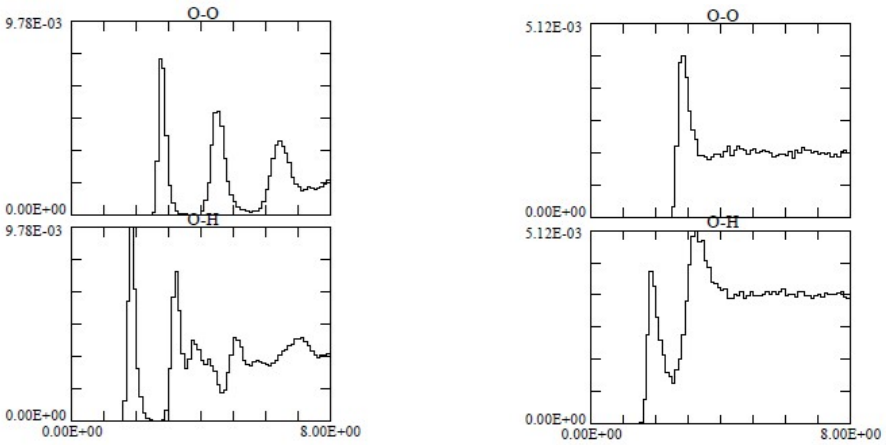

Figure 3: The pair distribution functions between the O-O atoms (top) and O-H atoms (bottom) of the methane hydrate for the density 0.91 g/cm^3. The time is before the collapse at $t = 1.65 \times 10^6 \tau$ (left), and after the collapse at $t = 1.70 \times 10^6 \tau$ (right). The three peaks for the O-O atoms show that the atoms have almost aggregated by the collapse in the right panel, and the two giant peaks indicate the O-H atoms.

around $\tau \cong 1.7 \times 10^6 \tau_0$. Well separated peaks in the 8 Å regions can be identified as a crystal before the collapse on the top and bottom panels of the left side. However, one has only one peak as liquid after the collapse, which is entirely buried in the $r > 3$ Å region of the O-O distribution function. Two peaks are seen with curtains in the O-H functions of the right panel.

The external electric field is made large as $E = 0.4$ V/Å in Run A2 of Table 1. The heating rate becomes very large $3.7 \times 10^{-5} W_0/\tau$, and there is a short nonlinear phase before its collapse at $t \cong 6.3 \times 10^4 \tau$.

4 Summary

Methane hydrate was simulated by molecular dynamics with periodic boundary conditions. The normal density of 0.91 g/cm^3 represented sea level conditions. The microwave electric field was applied while the volume was held constant. For Run A1, the external electric field was $E = 0.30$V/Å and the heating rate was $3.0 \times 10^{-7} W_0/\tau$. The methane hydrate collapsed to be liquid for the normal density, and the temperature increase before the collapse occured at $t \cong 1.7 \times 10^6 \tau$, and the temperture increase was $\Delta T \cong 61$ degrees. For Run A2 of $E = 0.40$ V/Å, the heating rate was very large $3.7 \times 10^{-5} W_0/\tau$, and methane hydrate collapsed shortly at $t \cong 6.3 \times 10^4 \tau$.

Acknowledgments

The author (M.T.) is grateful to Dr. M. Matsumote of Okayama University for the initial configuration of methane hydrate. The computation is performed by the NEC SX-Aurora TSUBASA of National Institute of Fusion Science, Japan.

Appendix A: Long-range Coulombic Interactions

The $G(n_x, n_y, n_z)$, $\vec{K}(n_x, n_y, n_z)$ and $\Delta(n_x, n_y, n_z)$ functions for the long-range Coulombic interactions are written in the periodic boundary conditions as,

$$G(n_x, n_y, n_z) = (2M_x M_y M_z / L^2) \times \Big[dn(n_x) K_x + dn(n_y) K_y + dn(n_z) K_z \Big] / (\Lambda \Delta^2), \tag{A.1}$$

$$\vec{K}(n_x, n_y, n_z) = \sum_{n_1, n_2, n_3} (n_1, n_2, n_3) \Big\{ \exp\Big(-\Big(\pi / (\alpha L) \Big)^2 \Big) / \Lambda \Big\} \times \Big(sinc\Big(\frac{n_x + M_x n_1}{M_x} \Big) \Big)^{2P} \Big(sinc\Big(\frac{n_y + M_y n_2}{M_y} \Big) \Big)^{2P} \Big(sinc\Big(\frac{n_z + M_z n_3}{M_z} \Big) \Big)^{2P} \tag{A.2}$$

$$\Delta(n_x, n_y, n_z) = \sum_{n_1, n_2, n_3} \Big(sinc\Big(\frac{n_x + M_x n_1}{M_x} \Big) \Big)^{2P} \times \Big(sinc\Big(\frac{n_y + M_y n_2}{M_y} \Big) \Big)^{2P} \Big(sinc\Big(\frac{n_z + M_z n_3}{M_z} \Big) \Big)^{2P}, \tag{A.3}$$

$$\Lambda = dn(n_x)^2 + dn(n_y)^2 + dn(n_z)^2. \tag{A.4}$$

The first Brillouin zone should take the summation of $-1 \leq n_1 \leq 1$ (the degree is $P = 3$), and M_x is the mesh in the x direction; the same procedures should be taken in the other directions due to the tetragonal crystal symmetry. The sinc function is used to account for the long slopes of the $\vec{K}(n_x, n_y, n_z)$ and $\Delta(n_x, n_y, n_z)$ functions. The index ranges for the $G(n_x, n_y, n_z)$ function are $0 \leq n_x \leq M_x/2$, $0 \leq n_y \leq M_y - 1$ and $0 \leq n_z \leq M_z - 1$, where M_x, M_y, and M_z are the number of points in the x, y, and z directions, respectively.

References

[1] E. D. Sloan, C. A. Koh, C. Koh, Clathrate Hydrates of Natural Gases, Third Edition, CRC Press (2007).

[2] A. A. Pavlov, J. F. Kastine, L. L. Brown, K. A. Rages, and R. Freedman, J. Geophys. Res., 105, 981-990 (2000).

[3] United State Environmental Protection Agency, Greenhouse Gas Emissions, https://www.epa.gov/ghgemissions/overview-greenhouse-gases.

[4] Methane hydrate mineral data, The Hudson Institute of Mineralogy, http://webmineral.com/data/Methane.

[5] H. Hirai, T. Tanaka, T. Kawamura, Y. Yamamoto, and T. Yagi, Phys. Rev. B, 68, 172102 (2003).

[6] O. S. Subbotin, T. Ikeshoji, V. R. Belosludov, J. Kudoh, R. V. Belosludov, and Y. Kawazoe, J. Physics Conference Series 29, 206 (2006).

[7] G. Soave, Chem. Eng. Sci. 27, 1197 (1972).

[8] A. Lucia, J. Thermodyn., Article id: 238365 (2010).

[9] H. Henley, E. Thomas, and A. Lucia, 92, 1977 (2014).

[10] T. Yamaguchi, S. H. Chong, and F. Hirata, J. Chem. Phys. 116, 2502 (2002).

[11] N. J. English and J. M. MacElroy, J. Chem. Phys. 118, 1589 (2003).

[12] M. Matsumoto, S. Saito and I. Ohmine , Nature, vol. 416, 409 (2002).

[13] M.Tanaka and M.Sato, J.Chem.Phys., 126, 034509 (2007).

[14] M.Tanaka and M.Sato, JMPEE, 42, 62-69 (2008).

[15] J. Izquierdo, A. Vega, L. Balbas, D. Sanchez-Portal, J. Junquera, E. Artacho, J. Soler, and P. Ordejon, Phys. Rev. B. 61, 13639 (2000).

[16] C. Kittel, Introduction to Solid State Physics, Six Edition (Willey, New York 1986).

[17] M. Tanaka and M. Murakami, Computer Physics Commun., 241, 56 (2019).

[18] P. Ewald, Ann. Phys. 369, 253 (1921).

[19] J. Kolafa, and J. W. Perram, Molecular Simulation. 9, 351 (1992).

[20] D. Frenkel and B. Smit, Understanding Molecular Simulation - From Algorithms to Applications, 2nd edition, Academic Press, United Kingdom, 2001.

[21] M. Deserno and C. Holm, J. Chem. Phys. 109, 7694 (1998).

[22] S.W. Rick, J. Chem. Phys. 120, 6085–6093 (2004).

[23] "Classical Mechanics", H. Goldstein, C. Poolee, J. Safko, 3rd Edition, Pearson Education Inc., England, 2003.

[24] H.C. Andersen, J. Comp. Physics, 52, 24-34 (1983).

[25] H.J.C. Berendsen, J.R. Grigera, T.P. Straatsma, J. Phys. Chem., 91, 6269 (1987)

[26] W.L. Jorgensen, J. Chandrasekhar, J.D. Madura, R.W. Impey, and M.R. Klein, J. Chem. Phys 79, 926 (1983).

[27] T.Okabe, H.Yamada and M.Goda, Int. J. Mod. Phys. C, 7. 613 (1996).

[28] M. Tanaka, M. Sato, and S. Nakatani, arXiv.1909.01024, Cornell University (2019).

[29] M. Matsumoto, T. Yagasaki, H. Tanaka, "GenIce: Hydrogen-Disordered Ice Generator", Wiley online, https://doi.org/10.1002/jcc.25077.

[30] A. Venkattraman and A. A. Alexeenko, Physics Fluids, 24, 027101 (2012).